Nonlocal quasinormal modes for arbitrarily shaped three-dimensional plasmonic resonators

Kamandar Dezfouli, Mohsen; Tserkezis, Christos; Mortensen, N. Asger; Hughes, Stephen

Published in:
Optica

Link to article, DOI:
10.1364/OPTICA.4.001503

Publication date:
2017

Document Version
Publisher's PDF, also known as Version of record

Research Article Vol. 4, No. 12 / December 2017 / Optica 1503

Nonlocal quasinormal modes for arbitrarily shaped three-dimensional plasmonic resonators

Mohsen Kamandar Dezfouli,[1,*] Christos Tserkezis,[2,3] N. Asger Mortensen,[2,3,4] and Stephen Hughes[1]

[1]Department of Physics, Engineering Physics and Astronomy, Queen's University, Kingston, Ontario K7L 3N6, Canada
[2]Department of Photonics Engineering, Technical University of Denmark, Ørsteds Plads, 343, DK-2800 Kgs. Lyngby, Denmark
[3]Center for Nano Optics, University of Southern Denmark, Campusvej 55, DK-5230 Odense M, Denmark
[4]Danish Institute for Advanced Study, University of Southern Denmark, Campusvej 55, DK-5220 Odense M, Denmark
*Corresponding author: m.kamandar@queensu.ca

Received 29 September 2017; revised 10 November 2017; accepted 13 November 2017 (Doc. ID 308257); published 4 December 2017

Nonlocal effects have been shown to be responsible for a variety of nontrivial optical effects in small-size plasmonic nanoparticles, beyond classical electrodynamics. However, it is not clear whether optical mode descriptions can be applied to such extreme confinement regimes. Here, we present a powerful quasinormal mode description of the nonlocal optical response for three-dimensional plasmonic nanoresonators. The nonlocal hydrodynamical model and a generalized nonlocal optical response model for plasmonic nanoresonators are used to construct an intuitive modal theory and to compare to the local Drude model response theory. Using the example of a gold nanorod, we show how an efficient quasinormal mode picture is able to accurately capture the blueshift of the resonances, the higher damping rates in plasmonic nanoresonators, and the modified spatial profile of the plasmon quasinormal modes, even at the single mode level. We exemplify the use of this theory by calculating the Purcell factors of single quantum emitters, the electron energy loss spectroscopy spatial maps, and the Mollow triplet spectra of field-driven quantum dots with and without nonlocal effects for different size nanoresonators. Our nonlocal quasinormal mode theory offers a reliable and efficient technique to study both classical and quantum optical problems in nanoplasmonics.

OCIS codes: (240.6680) Surface plasmons; (160.4236) Nanomaterials; (270.0270) Quantum optics.

https://doi.org/10.1364/OPTICA.4.001503

1. INTRODUCTION

Fundamental studies of light-matter interactions using plasmonic devices continue to make considerable progress and offer a wide range of applications [1–7]. For spatial positions very close to metal resonators, the local Drude model is known to fail, which challenges many of the usual modeling techniques that use the classic Maxwell equations. In particular, charge density oscillations become relevant, causing frequency shifts of the localized surface plasmon (LSP) resonance, as well as the appearance of additional resonances above the plasmon frequency [8–13]. Such investigations have been performed using both density functional theory (DFT) at the atomistic level [14] and using macroscopic nonlocal Maxwell's equations in the form of the hydrodynamical model (HDM) [13] and a generalized nonlocal optical response (GNOR) model [15]. However, so far, with the exception of the simple cases of spherical or cylindrical nanoparticles, nonlocal investigations have been primarily done using purely numerical simulations [16–18], which is not only computationally very expensive for arbitrary shaped plasmonic systems but can also lack important physical insight; most of these calculations are also restricted to 2D geometries or simple particle shapes. Thus, there is now a need for more intuitive and efficient formalisms with nonlocal effects included, for arbitrarily shaped metal resonators in a numerically feasible way.

In optics and nanophotonics, one of the most successful analytical approaches to most resonator problems is to adopt a modal picture of the optical cavity (e.g., in cavity-QED and coupled mode theory). Recently, it has been also shown that quasinormal modes (QNMs) can quantitatively describe the dissipative modes of both dielectric cavities and LSP resonances [19] and even hybrid structures of metals and photonic crystals [20]. In contrast to "normal modes," which are solutions to Maxwell's equations subjected to (usually) fixed or periodic boundary conditions, QNMs are obtained with open boundary conditions [21], and they are associated with complex frequencies whose imaginary parts quantify the system losses. These QNMs require a more generalized normalization [21–26], allowing for accurate mode quantities to be obtained such as the effective mode volume or Purcell factor [27], that is, the enhanced spontaneous emission (SE) factor of a dipole emitter. These QNMs are typically computed numerically from the Helmholtz equation with open boundary conditions, for example, with perfectly matched layers (PMLs), whose solution

can then be used to construct the full photon Green function (GF) of the medium—a function that is well known to connect to many useful quantities in classical and quantum optics [28–38]. The GF can also be used (and indeed is required) to compute electron energy loss spectroscopy (EELS) maps for plasmonic nanostructures [39–50], which is a notoriously difficult problem in computational electrodynamics, especially for nanoparticles or arbitrary shape. Despite these successes with QNMs, in the presence of nonlocal effects, it is not known whether such a mode description even applies.

In this work, we show that, somewhat surprisingly, QNMs can indeed be obtained and used to construct the full system GF for complex 3D plasmonic nanoresonators with nonlocal effects, and even a single mode description is accurate over a wide range of frequencies and spatial positions. We start by redefining the Helmholtz equation that is usually solved to obtain the local QNMs [37], and then we extend this approach to the case of nonlocal systems using a generalized Helmholtz equation, which is applicable to both HDM and GNOR models. A semi-analytical modal GF is then used to perform Purcell factor calculations of dipole emitters positioned nearby plasmonic gold nanorods (a structure for which there is no known analytical GF). We then show the accuracy of the modal Purcell factors against fully vectorial dipole calculations, also computed in the presence of the nonlocal corrections. The calculated QNMs are also used to accurately quantify the effective mode volume associated with coupling to quantum emitters and can be used, for example, for quantifying single photon source figures of merit [6,51]. Additionally, we examine the size dependence of the nonlocal behavior by investigating nanorods of different sizes, verifying the anticipated LSP blueshifts [11], and damping with decreasing nanoparticle size [15]. Next, we use our QNM technique to efficiently calculate the EELS maps for different sizes of nanoparticles [40,47,48]. Finally, to more rigorously show the benefit of our nonlocal modal picture for use in quantum theory of light-matter interaction, we study the behavior of the Mollow triplets of field-driven quantum dots (QDs) coupled to plasmonic resonators [52], under the influence of nonlocal effects.

2. CAVITY MODE APPROACH TO NONLOCAL PLASMONICS

Without nonlocal corrections to the metal, the QNMs, $\tilde{\mathbf{f}}_\mu(\mathbf{r})$, can be defined as the solution to the Helmholtz equation with open boundary conditions (such as PMLs),

$$\nabla\times\nabla\times\tilde{\mathbf{f}}_\mu(\mathbf{r})-\left(\frac{\tilde{\omega}_\mu}{c}\right)^2\varepsilon(\mathbf{r},\omega)\tilde{\mathbf{f}}_\mu(\mathbf{r})=0, \tag{1}$$

where $\varepsilon(\mathbf{r},\omega)$ is the relative dielectric function of the system, and $\tilde{\omega}_\mu=\omega_\mu-i\gamma_\mu$ is the complex resonance frequency that can also be used to quantify the QNM quality factor, $Q_\mu=\omega_\mu/2\gamma_\mu$. For metallic regions, the dielectric function can be described using the local Drude model, $\varepsilon_{\mathrm{MNP}}(\mathbf{r},\omega)=1-\omega_p^2/\omega(\omega+i\gamma_p)$, with $\hbar\omega_p=8.29$ eV and $\hbar\gamma_p=0.09$ eV for the plasmon frequency and collision rate of gold [53], respectively. However, when considering the nonlocal nature of the plasmonic system, the electric field displacement relates to the electric field through an integral equation rather than a simple proportionality [12,54]. In this *nonlocal* case, a modified set of equations [13,15] can be used to define nonlocal QNMs, $\tilde{\mathbf{f}}_\mu^{\mathrm{nl}}(\mathbf{r})$, from

$$\nabla\times\nabla\times\tilde{\mathbf{f}}_\mu^{\mathrm{nl}}(\mathbf{r})-\left(\frac{\tilde{\omega}_\mu^{\mathrm{nl}}}{c}\right)^2\tilde{\mathbf{f}}_\mu^{\mathrm{nl}}(\mathbf{r})=i\tilde{\omega}_\mu^{\mathrm{nl}}\mu_0\mathbf{J}_\mu, \tag{2}$$

$$\xi^2\nabla[\nabla\cdot\mathbf{J}_\mu]+\tilde{\omega}_\mu^{\mathrm{nl}}(\tilde{\omega}_\mu^{\mathrm{nl}}+i\gamma_p)\mathbf{J}_\mu=i\tilde{\omega}_\mu^{\mathrm{nl}}\omega_p^2\varepsilon_0\tilde{\mathbf{f}}_\mu^{\mathrm{nl}}(\mathbf{r}), \tag{3}$$

where $\mathbf{J}_\mu$ is the induced current density and ξ is a phenomenological length scale associated with the nonlocal corrections [15]. Indeed, $\xi^2=\beta^2+D(\gamma_p-i\omega)$, where β is the hydrodynamic parameter proportional to the electron Fermi velocity, $v_{\mathrm{F}}=1.39\times10^6$ m/s, and $D=2.9\times10^{-4}$ m^2/s [55] is the diffusion constant associated with the short-range nonlocal response. While ξ in its full form represents the GNOR model, we can simply switch to the HDM by neglecting the diffusion.

Traditionally in cavity physics, the concept of effective mode volume, V_{eff}, plays a key role in characterizing the mode properties; historically, V_{eff} quantifies the degree of light confinement in optical cavities, and it is normally defined at the modal antinode where, for example, a quantum emitter is typically placed. Even though for plasmonic dimers one can reasonably choose the gap center as the place to calculate the mode volume, for plasmonic resonators in general, this simple picture of mode volume is ambiguous. However, one can still quantify an effective modal volume, $V_{\mathrm{eff}}^{\mathrm{nl}}(\mathbf{r})=\mathrm{Re}\{1/n_b^2[\tilde{\mathbf{f}}_\mu^{\mathrm{nl}}(\mathbf{r})]^2\}$ (same definition holds for the local QNM, only one uses $\tilde{\mathbf{f}}_\mu$) [19], for rigorous use in Purcell's formula, which is associated with coupling to emitters at different locations outside (but typically near) the metal nanoparticle within a background medium of refractive index n_b. Such a position-dependent mode volume can then be used in a generalized Purcell factor,

$$F_{\mathrm{P}}(\mathbf{r})=\frac{3}{4\pi^2}\left(\frac{\lambda_c}{n_b}\right)^3\frac{Q}{V_{\mathrm{eff}}(\mathbf{r})}, \tag{4}$$

to obtain the SE enhancement rate of a dipole emitter placed at $\mathbf{r}$ around a cavity with the resonance wavelength of λ_c and quality factor of Q. The quantum emitter is assumed to be on resonance and aligned in polarization with the LSP mode.

Recent work has shown that QNMs, when obtained in normalized form (as done in this work), accurately describe lossy plasmonic resonators using the local Drude model [20,37,56]. Here, we extend such an approach to include the nonlocal effects by introducing the expansion

$$\mathbf{G}_{\mathrm{sc}}^{\mathrm{nl}}(\mathbf{r}_1,\mathbf{r}_2;\omega)=\sum_\mu\frac{\omega^2}{2\tilde{\omega}_\mu^{\mathrm{nl}}(\tilde{\omega}_\mu^{\mathrm{nl}}-\omega)}\tilde{\mathbf{f}}_\mu^{\mathrm{nl}}(\mathbf{r}_1)\tilde{\mathbf{f}}_\mu^{\mathrm{nl}}(\mathbf{r}_2), \tag{5}$$

for the scattered GF, which is extremely useful, as it can be immediately used to obtain the full position and frequency dependence of the generalized Purcell factor (SE enhancement factor) for a dipole emitter polarized along $\mathbf{n}$: [32]

$$F(\mathbf{r};\omega)=1+\frac{6\pi c^3}{\omega^3 n_b}\mathbf{n}\cdot\mathrm{Im}\{\mathbf{G}_{\mathrm{sc}}^{\mathrm{nl}}(\mathbf{r},\mathbf{r};\omega)\}\cdot\mathbf{n}, \tag{6}$$

where we include a factor of 1 for emitters outside the resonator [37]. Note that in a single mode regime, if at the peak of the resonance frequency, $\omega=2\pi c/\lambda_c$, then Eq. (6) reduces to Eq. (4).

3. RESULTS AND EXAMPLE APPLICATIONS

In this section, a selection of applications are presented to demonstrate the power and reliability of the QNM theory for light-matter investigations of plasmonic resonators, into the

nonlocal regime. We emphasize that, once the QNMs are calculated, as discussed in subsection A, all example studies are performed in seconds, owing to the analytical power of the technique.

A. Local Versus Nonlocal Quasinormal Modes

To obtain the system QNMs for the nonlocal HDM/GNOR model defined via Eqs. (2) and (3), we employ the frequency domain technique discussed in Ref. [25] (used for the local Drude model), where an inverse GF approach is used to return the QNM in normalized form without having to carry out any spatial integral. We extend this method by incorporating nonlocal corrections, both for the HDM method [57], as well as the more complete GNOR model [15,58]. While the system GF using the notation of [25] finds a different form, for consistency, we follow the approach of Eq. (5) to briefly explain the technique.

The basic idea is to use a dipole excitation at the location of interest, $\mathbf{r}_0$, having a dipole moment of $\mathbf{d}$, to numerically obtain the scattered GF (as explained in more detailed later), $\mathbf{G}_{sc}(\mathbf{r}_0, \mathbf{r}_0; \omega)$, and then reverse Eq. (5) to obtain

$$\tilde{\mathbf{f}}_c(\mathbf{r}_0) \cdot \mathbf{d} = \sqrt{\frac{\mathbf{d} \cdot \mathbf{G}_{sc}(\mathbf{r}_0, \mathbf{r}_0; \tilde{\omega}_c) \cdot \mathbf{d}}{A(\tilde{\omega}_c)}}, \tag{7}$$

where a single QNM, $\tilde{\mathbf{f}}_c(\mathbf{r})$, with the complex frequency $\tilde{\omega}_c$ is considered, and we have defined $A(\omega) = \omega^2/2\tilde{\omega}_c(\tilde{\omega}_c - \omega)$ for convenience. The above quantity is in fact all one needs to perform an integration-free normalization for the QNM, and in practice, it is calculated at frequencies very close to the QNM frequency [so is the QNM of Eq. (8)] [25]. When inserted back into Eq. (5), one arrives at

$$\tilde{\mathbf{f}}_c(\mathbf{r}) = \frac{\mathbf{G}_{sc}(\mathbf{r}, \mathbf{r}_0; \tilde{\omega}_c) \cdot \mathbf{d}}{\sqrt{A(\tilde{\omega}_c)[\mathbf{d} \cdot \mathbf{G}_{sc}(\mathbf{r}_0, \mathbf{r}_0; \tilde{\omega}_c) \cdot \mathbf{d}]}}, \tag{8}$$

which provides the full spatial profile of the QNM, given that one also keeps track of the system response at all other locations, $\mathbf{G}_{sc}(\mathbf{r}, \mathbf{r}_0; \omega)$, within the same simulation.

The numerical implementation is done using the frequency domain finite-element solver COMSOL [59], where an electric current dipole source is used to excite the system and iteratively search for the QNM frequencies by monitoring the strength of the system response [25]. To obtain the QNM, one obtains the scattered GF as the difference between two dipole simulation GFs at frequencies very close to the QNM frequency, with and without the metal nanoparticles [25], either in local or nonlocal case. The computed QNM can then provide the full spectral and spatial shape of the resonances involved. In our calculations, a computational domain of 0.5 μm^3 was used for all simulations with a maximum element size of 0.2 nm on the nanoparticle surface and 0.6 nm inside. The maximum element size elsewhere is set to 33 nm to ensure convergent results over a wide range of frequencies, and 10 layers of PML were used. We have checked that these parameters provide accurate numerical convergence for both local and nonlocal simulations done in this work.

Depicted in Fig. 1 are the computed QNMs for three different gold cylindrical nanorods with the same aspect ratio, varying from 20 nm to 4 nm in length (see figure caption for details). The left panels represent the local Drude model QNMs, while the right panels show the QNMs using the nonlocal GNOR model. As seen, the main QNM shapes are similar but a redistribution of the localized field clearly occurs due to the inclusion of the nonlocal corrections. While the local Drude model predicts a similar mode shape for the different nanoparticle sizes, the nonlocal corrections introduce a pronounced degree of mode reshaping for smaller nanoparticles. Indeed, even for the largest nanoparticle shown in Figs. 1(a) and 1(b), higher field values are seen both inside as well as outside (but near) the metallic region.

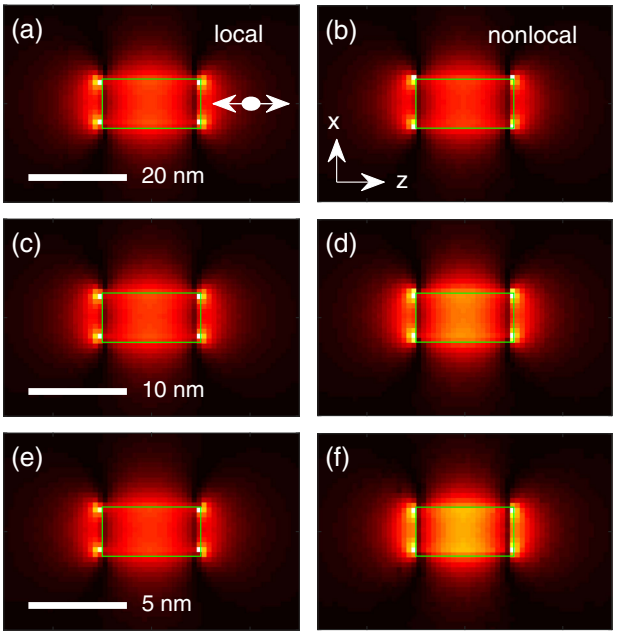

Fig. 1. Comparison between the local QNM (a, c, e), $|\tilde{\mathbf{f}}(x, z, y_0)|^2$ and nonlocal GNOR QNM (b, d, f), $|\tilde{\mathbf{f}}^{nl}(x, z, y_0)|^2$ for nanorods of different heights, $h = 20$ nm, $h = 10$ nm, and $h = 5$ nm, where $y_0 = 0$ is at the center of the nanorods. Same geometrical aspect ratio of 2 is used corresponding to a radius of $r = 5$ nm for the largest resonator. Double arrow in (a) shows the location of the dipole emitter at 10 nm away from the metallic surface that is kept the same for all QNM calculations, and the green box represents the metallic border.

B. Purcell Factors from Coupled Dipole Emitters

Figure 2 shows the computed QNM Purcell factors using the local Drude model and the two different nonlocal models for the $h = 20$ nm nanorod. As can be seen, both HDM and GNOR models predict the known blueshift of the plasmonic resonance [12–14]. However, the nonlocal prediction of the peak enhancement strongly depends on the model chosen. The GNOR model, in particular, predicts a considerably lower Purcell factor due to the inclusion of diffusion, which accounts for surface-enhanced Landau damping [15]. Indeed, as will be discussed shortly, including the nonlocal effects modifies both the quality factor and the mode volume associated with QNMs. The inset also shows the validity of our Purcell factor calculations against full dipole numerical calculations, only shown here for the nonlocal GNOR response. However, a similar degree of very good agreement is observed for all other calculations both in Fig. 2 and what follows.

In Fig. 2, in the bottom panel, we additionally plot the corresponding effective mode volume for a range of dipole locations, from the nanorod surface (at $z = 10$ nm) up to 10 nm away. A comparison between the local Drude model (solid-blue) and the nonlocal GNOR (dashed-red) is shown, where a nontrivial difference is observed. Closer to the metallic surface, smaller

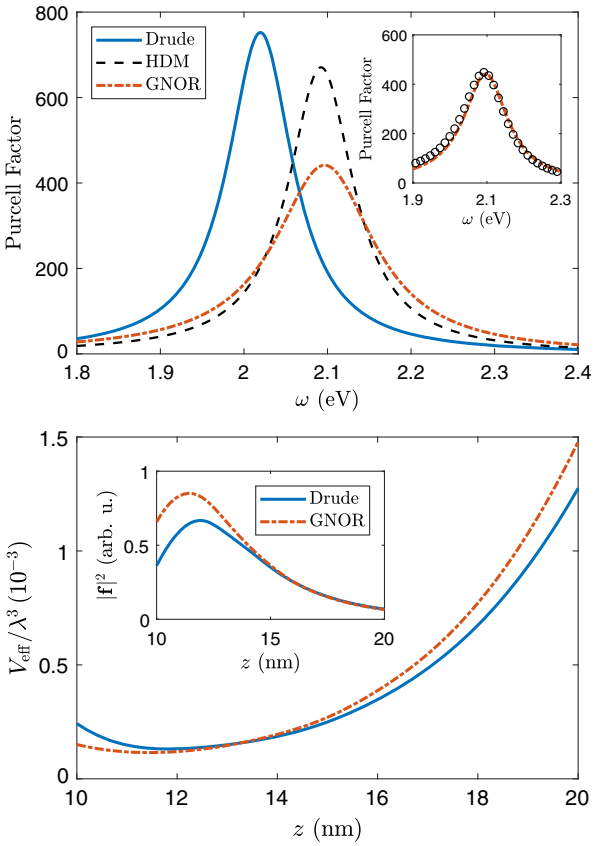

Fig. 2. Top: generalized Purcell factor for a dipole emitter placed 10-nm away form a gold nanorod of height $h = 20$ nm and radius of $r = 5$ nm, using Drude QNM, nonlocal HDM QNM, and nonlocal GNOR QNM. The inset shows the agreement between full dipole calculations (with no approximations) and GNOR QNM results. Bottom: corresponding QNM effective mode volume, V_{eff}, is shown for a range of locations above the nanorod. Note that $z = 10$ nm is at the surface of the metallic nanoparticle. Inset shows the modal absolute magnitude for completeness.

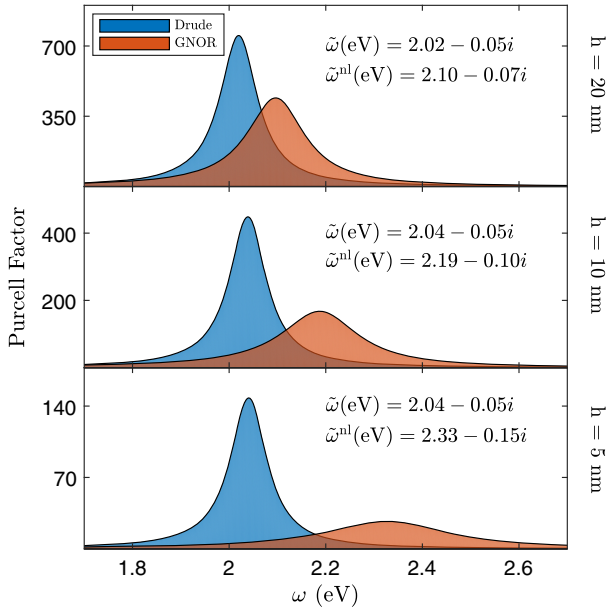

Fig. 3. Size-dependent discrepancy in Purcell factor between the local Drude model and nonlocal GNOR model. Results are derived from analytical QNM calculations when the dipole emitter is kept 10-nm away along the z-axis. Complex resonance frequencies for both models are also shown in each case.

effective mode volumes are predicted by the nonlocal corrections, while further away, the opposite takes place. The difference at larger distances, however, is mainly due to nonlocal corrected resonant wavelengths that are used to normalize the mode volumes.

We also consider enhanced SE from the three different gold nanoparticles discussed in Fig. 1. Plotted in Fig. 3 are the QNM calculations of the Purcell factors for dipole emitters located 10-nm away from nanorods, on the z-axis. In each case, the local Drude results are compared with the nonlocal GNOR results. Clearly, nonlocal corrections result in larger resonance blueshifts and larger damping rates (lower quality factors).

C. Computing EELS Spatial Maps

For our next application of the nonlocal QNM theory, we calculate the spatial maps associated with EELS experiments that are obtained by nanometer-scale resolution in microscopy of LSP resonances [40,41,44,49,50]. Since the GF is available at all locations (near the resonator) through QNM expansion of Eq. (5), the EELS spectra in the xz plane subjected to an electron beam propagating along the y axis can be easily obtained from [40,48]

$$\Gamma(x, z; \omega) = -\frac{4e^2 v^2}{\hbar} \int \mathrm{d}t\mathrm{d}t' \,\mathrm{Im}\{e^{i\omega(t'-t)} G_{yy}(\mathbf{r}_e(t), \mathbf{r}_e(t'); \omega)\}, \tag{9}$$

where v is the speed of electrons, and the single mode expansion for our Green function—that is already confirmed to be very accurate—is used. The EELS calculations for all three nanoparticles (of Fig. 1) are shown in Fig. 4, all computed at the

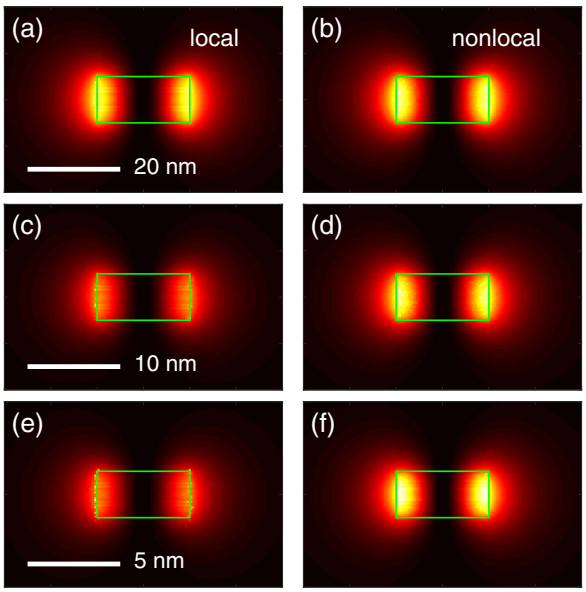

Fig. 4. Comparison between the EELS map of the plasmonic nanorod using the local Drude model, (a, c, e) and nonlocal GNOR model, (b, d, f), where each map is calculated at the corresponding plasmonic peak frequency. Same geometries as in Fig. 1 are used, and green box represents the metallic border.

corresponding plasmonic peak frequencies. Note that there are some noticeable numerical issues around the sharp corners of the metallic nanorod when using the conventional Drude model theory on the left (which is a known problem [60,61]). Using the same meshing scheme, however, the nonlocal description evidently helps to avoid such nonphysical effects. More importantly, as the nanoparticle size decreases, the EELS map becomes brighter at the maximum location which originates from the higher modal amplitudes of the QNMs discussed in Fig. 1. We stress again that with the computed QNMs, such EELS maps are calculated instantaneously, which is a far cry from the many brute force numerical solvers.

D. Field-Driven Mollow Triplets and Quantum Optics Regime

Finally, in addition to the previous discussions on Purcell factor and mode volume that are important for building quantum optical models of light-matter interaction [62], we discuss the quantum regime of field-driven Mollow triplets for QDs coupled to plasmonic nanoparticles. In the dipole and rotating wave approximations, the total Hamiltonian of the coupled system is [52,63]

$$H = \hbar \int \mathrm{d}\mathbf{r} \int_0^\infty \mathrm{d}\omega \omega \hat{\mathbf{f}}^\dagger(\mathbf{r},\omega)\hat{\mathbf{f}}(\mathbf{r},\omega) + \hbar\omega_x \sigma^+\sigma^- - \left[\sigma^+ \int_0^\infty \mathrm{d}\omega \mathbf{d}\cdot\hat{\mathbf{E}}(\mathbf{r}_d,\omega) + \mathrm{H.c.}\right] + \frac{\hbar\Omega}{2}(\sigma^+ e^{-i\omega_L} + \sigma^- e^{i\omega_L}), \tag{10}$$

where $\Omega = \langle \hat{\mathbf{E}}_{\mathrm{pump}}(\mathbf{r}_d)\rangle \cdot \mathbf{d}/\hbar$ is the effective Rabi field, σ^+, σ^- are the Pauli operators of the two-level atom (or exciton), ω_x is the resonance of the exciton, $\mathbf{d}$ is the dipole of the exciton, and $\hat{\mathbf{f}}, \hat{\mathbf{f}}^\dagger$ are the boson field operators. Following the approach in Ref. [52] and using the interaction picture at the laser frequency ω_L, one can derive a self-consistent generalized master equation in the 2nd-order Born–Markov approximation:

$$\frac{\partial\rho}{\partial t} = \frac{1}{i\hbar}[H_S,\rho] + \int_0^t \mathrm{d}\tau\{\tilde{J}_{\mathrm{ph}}(\tau)[-\sigma^+\sigma^-(-\tau)\rho + \sigma^-(-\tau)\rho\sigma^+] + \mathrm{H.c.}\}, \tag{11}$$

where $\tilde{J}_{\mathrm{ph}}(\tau) = \int_0^\infty \mathrm{d}\omega J_{\mathrm{ph}}(\omega) e^{i(\omega_L-\omega)\tau}$, with the photon-reservoir spectral function given by $J_{\mathrm{ph}}(\omega) \equiv \frac{\mathbf{d}\cdot\mathrm{Im}[\mathbf{G}(\mathbf{r}_d,\mathbf{r}_d;\omega)]\cdot\mathbf{d}}{\pi\hbar\varepsilon_0}$, and the time-dependent operators are defined through $\sigma^\pm(-\tau) = e^{-iH_S\tau/\hbar}\sigma^\pm e^{iH_S\tau/\hbar}$, with $H_S = \hbar(\omega_x-\omega_L)\sigma^+\sigma^- + \hbar\Omega/2(\sigma^+ + \sigma^-)$, which results in a complex interplay between the values of the local density of states at the field-driven dressed states. Solving the master equation and exploiting the quantum regression theorem, one can compute the incoherent spectrum of the QD emission from [52]

$$S_0(\omega) = \lim_{t\to\infty} \mathrm{Re}\left[\int_0^\infty \mathrm{d}\tau(\langle\sigma^+(t-\tau)\sigma^-(t)\rangle - \langle\sigma^+(t)\rangle\langle\sigma^-(t)\rangle)e^{i(\omega_L-\omega)\tau}\right], \tag{12}$$

as well as the detected spectrum, which includes quenching and propagation from QD at $\mathbf{r}_0$ to a point detector at $\mathbf{r}_D$, from [52]

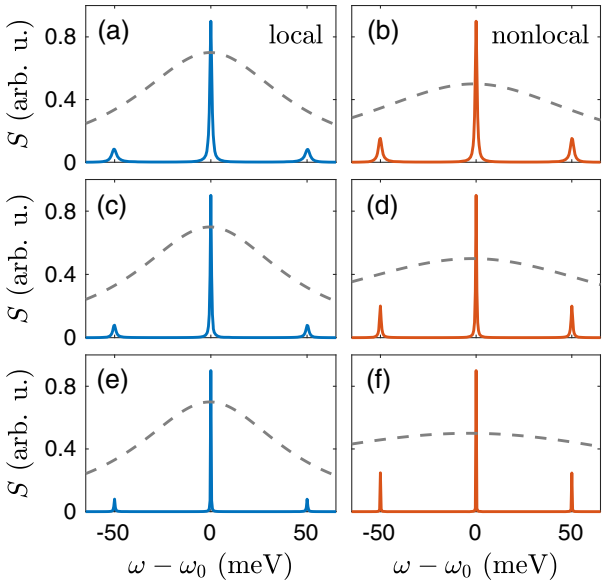

Fig. 5. Detected spectra (S evaluated at $\mathbf{r}_D = 200$ nm) of a field-driven QD coupled to plasmonic nanoparticles, where the same ordering of the particle size and QD location as in Fig. 1 is followed, and we use an effective Rabi field of $\Omega = 50$ meV. Plasmonic enhancement is also shown in dashed-gray in background. Nonlocal investigations on the right predict relatively stronger side peaks for the Mollow triplet with narrower linewidths.

$$S(\mathbf{r}_D;\omega) = \frac{2}{\varepsilon_0}|\mathbf{G}(\mathbf{r}_D,\mathbf{r}_0;\omega)\cdot\mathbf{d}|^2 S_0(\omega). \tag{13}$$

For example calculations, we assume a QD with the dipole moment of $|\mathbf{d}| = 50$ Debye at 10-nm away from the nanoparticle surface, at $x = 0$. In particular, as with the calculations above, we compare the local Drude model versus the nonlocal GNOR model, as shown in Fig. 5. As can be recognized, including the nonlocal effects, in general, predicts narrower linewidths for the Mollow triplets (see Table 1), where the relative strength of the side peaks are also increased. This is attributed to the modified plasmonic enhancement in the nonlocal description as confirmed in Fig. 3, which can be also rigorously confirmed using analytical equations for the linewidths derived in Ref. [52]. It should be noted that, in general, the detected spectrum S for the Mollow triplet problem can be different than the emitted S_0, as discussed in Ref. [52]; however in our particular case, under the resonant excitation, we find that they have the same qualitative shape (and differ only quantitatively). We also stress that these spectral calculations, at any detector position, can be trivially performed using a standard desktop through use of semi-analytical GF of

Table 1. Linewidth of the Central Mollow Peak for the Three Nanoparticles, Using Both Drude Model and GNOR Model[a]

h (nm)	Drude FWHM (meV)	GNOR FWHM (meV)
20	1.28	1.21
10	0.74	0.61
5	0.45	0.42

[a]Same trend holds for the side peaks.

Eq. (5), demonstrating the power of our approach for carrying out complex problems in quantum optics.

4. CONCLUSIONS

We have presented an efficient and accurate modal description of the nonlocal response of arbitrarily shaped metallic nanoparticles, using a fully 3D model. We have shown how semi-analytical nonlocal QNMs can be used to accurately construct the system GF from which modal quantities of interest such as Purcell factor and effective mode volume can be derived. As anticipated, we first observe the blueshift, as well as the larger damping rate for the LSP as a consequence of nonlocal effects. We further confirmed the validity of our approach for different nanoparticle sizes with full dipole solutions of the modified Maxwell equations, allowing us to predict the size-dependent nonlocal modifications with ease. As example applications of the theory, we described how our nonlocal QNMs can be used to efficiently model Purcell factors of quantum dipole emitters, EELS spatial maps, and Mollow triplet spectra of field-driven QD. The presented model has many applications in both classical and quantum nanoplasmonics, offers considerable analytical insight into complex nonlocal problems, and could help pave the way for a quantum description of both light and matter in nonlocal coupling regimes.

Funding. Natural Sciences and Engineering Research Council of Canada (NSERC); Queen's University; FP7 People: Marie-Curie Actions (PEOPLE) (609405, COFUNDPostdocDTU); Villum Fonden (16498); Danish National Research Council (DNRF103).

REFERENCES

1. C. Ciracì, R. T. Hill, J. J. Mock, Y. Urzhumov, A. I. Fernández-Domínguez, S. A. Maier, J. B. Pendry, A. Chilkoti, and D. R. Smith, "Probing the ultimate limits of plasmonic enhancement," Science **337**, 1072–1074 (2012).
2. K. J. Savage, M. M. Hawkeye, R. Esteban, A. G. Borisov, J. Aizpurua, and J. J. Baumberg, "Revealing the quantum regime in tunnelling plasmonics," Nature **491**, 574–577 (2012).
3. R. Esteban, A. G. Borisov, P. Nordlander, and J. Aizpurua, "Bridging quantum and classical plasmonics with a quantum-corrected model," Nat. Commun. **3**, 825 (2012).
4. M. Pelton, "Modified spontaneous emission in nanophotonic structures," Nat. Photonics **9**, 427–435 (2015).
5. M. Barbry, P. Koval, F. Marchesin, R. Esteban, A. G. Borisov, J. Aizpurua, and D. Sánchez-Portal, "Atomistic near-field nanoplasmonics: reaching atomic-scale resolution in nanooptics," Nano Lett. **15**, 3410–3419 (2015).
6. T. B. Hoang, G. M. Akselrod, and M. H. Mikkelsen, "Ultrafast room-temperature single photon emission from quantum dots coupled to plasmonic nanocavities," Nano Lett. **16**, 270–275 (2016).
7. S. I. Bozhevolnyi and N. A. Mortensen, "Plasmonics for emerging quantum technologies," Nanophotonics **6**, 1185–1188 (2017).
8. R. Ruppin, "Optical properties of a plasma sphere," Phys. Rev. Lett. **31**, 1434–1437 (1973).
9. R. Fuchs and F. Claro, "Multipolar response of small metallic spheres: nonlocal theory," Phys. Rev. B **35**, 3722–3727 (1987).
10. P. T. Leung, "Decay of molecules at spherical surfaces: nonlocal effects," Phys. Rev. B **42**, 7622–7625 (1990).
11. F. J. García de Abajo, "Nonlocal effects in the plasmons of strongly interacting nanoparticles, dimers, and waveguides," J. Phys. Chem. C **112**, 17983–17987 (2008).
12. J. M. McMahon, S. K. Gray, and G. C. Schatz, "Nonlocal optical response of metal nanostructures with arbitrary shape," Phys. Rev. Lett. **103**, 097405 (2009).
13. S. Raza, G. Toscano, A.-P. Jauho, M. Wubs, and N. A. Mortensen, "Unusual resonances in nanoplasmonic structures due to nonlocal response," Phys. Rev. B **84**, 121412 (2011).
14. T. V. Teperik, P. Nordlander, J. Aizpurua, and A. G. Borisov, "Robust subnanometric plasmon ruler by rescaling of the nonlocal optical response," Phys. Rev. Lett. **110**, 263901 (2013).
15. N. A. Mortensen, S. Raza, M. Wubs, T. Søndergaard, and S. I. Bozhevolnyi, "A generalized non-local optical response theory for plasmonic nanostructures," Nat. Commun. **5**, 3809 (2014).
16. A. Wiener, A. I. Fernández-Domínguez, A. P. Horsfield, J. B. Pendry, and S. A. Maier, "Nonlocal effects in the nanofocusing performance of plasmonic tips," Nano Lett. **12**, 3308–3314 (2012).
17. L. Stella, P. Zhang, F. J. García-Vidal, A. Rubio, and P. García-González, "Performance of nonlocal optics when applied to plasmonic nanostructures," J. Phys. Chem. C **117**, 8941–8949 (2013).
18. R. Filter, C. Bösel, G. Toscano, F. Lederer, and C. Rockstuhl, "Nonlocal effects: relevance for the spontaneous emission rates of quantum emitters coupled to plasmonic structures," Opt. Lett. **39**, 6118–6121 (2014).
19. P. T. Kristensen and S. Hughes, "Modes and mode volumes of leaky optical cavities and plasmonic nanoresonators," ACS Photon. **1**, 2–10 (2014).
20. M. Kamandar Dezfouli, R. Gordon, and S. Hughes, "Modal theory of modified spontaneous emission for a hybrid plasmonic photonic-crystal cavity system," Phys. Rev. A **95**, 013846 (2017).
21. P. T. Leung, S. Y. Liu, S. S. Tong, and K. Young, "Time-independent perturbation-theory for quasi-normal modes in leaky optical cavities," Phys. Rev. A **49**, 3068–3073 (1994).
22. P. T. Kristensen, C. P. Van Vlack, and S. Hughes, "Generalized effective mode volume for leaky optical cavities," Opt. Lett. **37**, 1649–1651 (2012).
23. C. Sauvan, J. P. Hugonin, I. S. Maksymov, and P. Lalanne, "Theory of the spontaneous optical emission of nanosize photonic and plasmon resonators," Phys. Rev. Lett. **110**, 237401 (2013).
24. P. T. Kristensen, R. C. Ge, and S. Hughes, "Normalization of quasinormal modes in leaky optical cavities and plasmonic resonators," Phys. Rev. A **92**, 053810 (2015).
25. Q. Bai, M. Perrin, C. Sauvan, J.-P. Hugonin, and P. Lalanne, "Efficient and intuitive method for the analysis of light scattering by a resonant nanostructure," Opt. Express **21**, 27371–27382 (2013).
26. E. A. Muljarov and W. Langbein, "Exact mode volume and Purcell factor of open optical systems," Phys. Rev. B **94**, 235438 (2016).
27. E. M. Purcell, H. C. Torrey, and R. V. Pound, "Resonance absorption by nuclear magnetic moments in a solid," Phys. Rev. **69**, 37–38 (1946).
28. G. Ford and W. Weber, "Electromagnetic interactions of molecules with metal surfaces," Phys. Rep. **113**, 195–287 (1984).
29. J. E. Sipe, "New Green-function formalism for surface optics," J. Opt. Soc. Am. B **4**, 481–489 (1987).
30. G. S. Agarwal, "Anisotropic vacuum-induced interference in decay channels," Phys. Rev. Lett. **84**, 5500–5503 (2000).
31. M. Wubs, L. G. Suttorp, and A. Lagendijk, "Multiple-scattering approach to interatomic interactions and superradiance in inhomogeneous dielectrics," Phys. Rev. A **70**, 053823 (2004).
32. P. Anger, P. Bharadwaj, and L. Novotny, "Enhancement and quenching of single-molecule fluorescence," Phys. Rev. Lett. **96**, 113002 (2006).
33. S. Hughes and H. Kamada, "Single-quantum-dot strong coupling in a semiconductor photonic crystal nanocavity side coupled to a waveguide," Phys. Rev. B **70**, 195313 (2004).
34. V. S. C. Manga Rao and S. Hughes, "Single quantum dot spontaneous emission in a finite-size photonic crystal waveguide: proposal for an efficient 'On Chip' single photon gun," Phys. Rev. Lett. **99**, 193901 (2007).
35. C. Van Vlack, P. T. Kristensen, and S. Hughes, "Spontaneous emission spectra and quantum light-matter interactions from a strongly coupled quantum dot metal-nanoparticle system," Phys. Rev. B **85**, 075303 (2012).
36. W. Yan, N. A. Mortensen, and M. Wubs, "Green's function surface-integral method for nonlocal response of plasmonic nanowires in arbitrary dielectric environments," Phys. Rev. B **88**, 155414 (2013).
37. R. C. Ge, P. T. Kristensen, J. F. Young, and S. Hughes, "Quasinormal mode approach to modelling light-emission and propagation in nanoplasmonics," New J. Phys. **16**, 113048 (2014).
38. M. Kamandar Dezfouli and S. Hughes, "Quantum optics model of surface-enhanced Raman spectroscopy for arbitrarily shaped plasmonic resonators," ACS Photon. **4**, 1245–1256 (2017).

39. F. J. García De Abajo and M. Kociak, "Probing the photonic local density of states with electron energy loss spectroscopy," Phys. Rev. Lett. **100**, 106804 (2008).
40. D. Rossouw, M. Couillard, J. Vickery, E. Kumacheva, and G. A. Botton, "Multipolar plasmonic resonances in silver nanowire antennas imaged with a subnanometer electron probe," Nano Lett. **11**, 1499–1504 (2011).
41. O. Nicoletti, M. Wubs, N. A. Mortensen, W. Sigle, P. A. van Aken, and P. A. Midgley, "Surface plasmon modes of a single silver nanorod: an electron energy loss study," Opt. Express **19**, 15371–15379 (2011).
42. Z. Mohammadi, C. P. Van Vlack, S. Hughes, J. Bornemann, and R. Gordon, "Vortex electron energy loss spectroscopy for near-field mapping of magnetic plasmons," Opt. Express **20**, 15024–15034 (2012).
43. G. Boudarham and M. Kociak, "Modal decompositions of the local electromagnetic density of states and spatially resolved electron energy loss probability in terms of geometric modes," Phys. Rev. B **85**, 245447 (2012).
44. M. Husnik, F. Von Cube, S. Irsen, S. Linden, J. Niegemann, K. Busch, and M. Wegener, "Comparison of electron energy-loss and quantitative optical spectroscopy on individual optical gold antennas," Nanophotonics **2**, 241–245 (2013).
45. T. Christensen, W. Yan, S. Raza, A. P. Jauho, N. A. Mortensen, and M. Wubs, "Nonlocal response of metallic nanospheres probed by light, electrons, and atoms," ACS Nano **8**, 1745–1758 (2014).
46. S. Raza, S. Kadkhodazadeh, T. Christensen, M. Di Vece, M. Wubs, N. A. Mortensen, and N. Stenger, "Multipole plasmons and their disappearance in few-nanometre silver nanoparticles," Nat. Commun. **6**, 8788 (2015).
47. A. Hörl, A. Trügler, and U. Hohenester, "Full three-dimensional reconstruction of the dyadic green tensor from electron energy loss spectroscopy of plasmonic nanoparticles," ACS Photon. **2**, 1429–1435 (2015).
48. R.-C. Ge and S. Hughes, "Quasinormal mode theory and modelling of electron energy loss spectroscopy for plasmonic nanostructures," J. Opt. **18**, 054002 (2016).
49. R. G. Hobbs, V. R. Manfrinato, Y. Yang, S. A. Goodman, L. Zhang, E. A. Stach, and K. K. Berggren, "High-energy surface and volume plasmons in nanopatterned sub-10 nm aluminum nanostructures," Nano Lett. **16**, 4149–4157 (2016).
50. P. Shekhar, M. Malac, V. Gaind, N. Dalili, A. Meldrum, and Z. Jacob, "Momentum-resolved electron energy loss spectroscopy for mapping the photonic density of states," ACS Photon. **4**, 1009–1014 (2017).
51. I. Aharonovich, D. Englund, and M. Toth, "Solid-state single-photon emitters," Nat. Photonics **10**, 631–641 (2016).
52. R.-C. Ge, C. Van Vlack, P. Yao, J. F. Young, and S. Hughes, "Accessing quantum nanoplasmonics in a hybrid quantum dot-metal nanosystem: Mollow triplet of a quantum dot near a metal nanoparticle," Phys. Rev. B **87**, 205425 (2013).
53. R.-C. Ge and S. Hughes, "Design of an efficient single photon source from a metallic nanorod dimer: a quasi-normal mode finite-difference time-domain approach," Opt. Lett. **39**, 4235–4238 (2014).
54. J. M. McMahon, S. K. Gray, and G. C. Schatz, "Calculating nonlocal optical properties of structures with arbitrary shape," Phys. Rev. B **82**, 035423 (2010).
55. C. Tserkezis, J. R. Maack, Z. Liu, M. Wubs, and N. A. Mortensen, "Robustness of the far-field response of nonlocal plasmonic ensembles," Sci. Rep. **6**, 28441 (2016).
56. S. Axelrod, M. Kamandar Dezfouli, H. M. K. Wong, A. S. Helmy, and S. Hughes, "Hyperbolic metamaterial nanoresonators make poor single-photon sources," Phys. Rev. B **95**, 155424 (2017).
57. G. Toscano, S. Raza, A.-P. Jauho, N. A. Mortensen, and M. Wubs, "Modified field enhancement and extinction by plasmonic nanowire dimers due to nonlocal response," Opt. Express **20**, 4176–4188 (2012).
58. C. Tserkezis, N. Stefanou, M. Wubs, and N. A. Mortensen, "Molecular fluorescence enhancement in plasmonic environments: exploring the role of nonlocal effects," Nanoscale **8**, 17532–17541 (2016).
59. "COMSOL Multiphysics," https://www.comsol.com.
60. A. A. Sukhorukov, I. V. Shadrivov, and Y. S. Kivshar, "Wave scattering by metamaterial wedges and interfaces," Int. J. Numer. Model. **19**, 105–117 (2006).
61. H. Wallén, H. Kettunen, and A. Sihvola, "Surface modes of negative-parameter interfaces and the importance of rounding sharp corners," Metamaterials **2**, 113–121 (2008).
62. S. I. Bozhevolnyi and J. B. Khurgin, "The case for quantum plasmonics," Nat. Photonics **11**, 398–400 (2017).
63. S. Scheel, L. Knöll, and D.-G. Welsch, "Spontaneous decay of an excited atom in an absorbing dielectric," Phys. Rev. A **60**, 4094–4104 (1999).